Erschienen in: IEEE Journal of Photovoltaics ; 7 (2017), 1. - S. 91-96
https://dx.doi.org/10.1109/JPHOTOV.2016.2621342

Impact of Extended Contact Cofiring on Multicrystalline Silicon Solar Cell Parameters

Ana Peral, Amir Dastgheib-Shirazi, Vanesa Fano, Juan Carlos Jimeno, Giso Hahn, and Carlos del Cañizo

***Abstract*—During the temperature spike of the contact cofiring step in a solar cell process, it has been shown that the concentration of lifetime-killer dissolved metallic impurities increases, while adding an annealing after the spike getters most of the dissolved impurities toward the phosphorus emitter, where they are less detrimental. The contact cofiring temperature profile, including the after-spike annealing, has been called extended contact cofiring, and it has also been proposed as a means to decrease the emitter saturation current density of highly doped emitters, thus benefiting a wide range of materials in terms of detrimental impurity content. The aim of the present work is to determine the effect of performing this additional annealing on contact quality and solar cell performance, looking for an optimal temperature profile for reduction of bulk and emitter recombination without affecting contact quality. It presents the effect of the extended cofiring step on fill factor, series resistance, and contact resistance of solar cells manufactured with different extended cofiring temperature profiles. Fill factor decreases when extended cofiring is performed. Series resistance and contact resistance increase during annealing, and this happens more dramatically when the temperature peak is decreased. Scanning electron microscopic images show silver crystallites in contact with silver bulk before the annealing that allow a direct current path, and silver crystallites totally surrounded by glass layer ($>$100 nm thick) after annealing. Glass layer redistribution and thickening at low temperatures at the semiconductor–metal interface can be related to the series resistance increase. Degradation of series resistance during the temperature spike, when it is below the optimum one, can also be attributed to an incomplete silicon nitride etching and silver crystallite formation. To make full use of the beneficial effects of annealing, screen-printing metallic paste development supporting lower temperatures without a thick glass layer growth is needed.**

***Index Terms*—Cofiring step, contact formation, extended gettering, low thermal annealing.**

I. Introduction

CONTACT formation is the last step of conventional industrial silicon solar cell production. The state-of-the-art technology consists of printing metal-based pastes on top of the silicon nitride layer for the front side and on silicon for the bottom side, followed by a fast inline cofiring at high temperature. This cofiring temperature profile requires a drying step with temperatures below 400 °C for burning out the organic binders, a step with temperatures between 475 and 600 °C that melts the glass frit and sinters the silver, and a short spike with a temperature between 600 and 900 °C that etches the dielectric silicon nitride antireflection coating and facilitates the formation of silver crystallites on the silicon surface [1]–[4].

In addition, it has been experimentally demonstrated in previous works that during the contact cofiring step, the concentration of dissolved iron in the wafer bulk is increased, decreasing bulk lifetime. Predictive impurity-to-efficiency simulations [5], [6] show a relative increase of dissolved iron during the standard cofiring step between 200% and 1000% for materials with high total contamination concentration (with initial total Fe concentrations between 10^{15} and 10^{16} cm^{-3} and iron precipitate radii between 15 and 50 nm). This increase can be attributed to the dissolution of iron precipitates [5]–[7], as well as to the reinjection of iron from the emitter into the bulk [8], [9]. However, adequate defect engineering tools can compensate completely or partly this increase, thanks to an external gettering into the phosphorus and aluminum layers during the temperature plateau. A short annealing step (5 min) after the standard cofiring has been calculated to decrease dissolved iron concentration more than 100% (comparing with results after standard recipe) for the most part of the conventional commercial materials, including the highly contaminated ones. Due to the fact that the concept is somewhat similar to what is called extended gettering [10]–[12], it was called extended cofiring.

It must also be noted that an additional benefit of a low-temperature anneal comes from a reduction in the emitter saturation current density as compared with a process without annealing, as has been shown recently in [13].

This paper deals with the consequences of an extended cofiring step on solar cell performance. As a change in firing conditions might have consequences for contact formation in general and contact resistance in particular, we investigate the behavior of these parameters on the solar cell level and trace them back to their microscopic origin.

II. Extended Cofiring on Contaminated Multicrystalline Silicon

This section presents an example of how the cofiring temperature profile impacts bulk lifetime of multicrystalline material, but other factors should be taken into account for that to be reflected in solar cell performance.

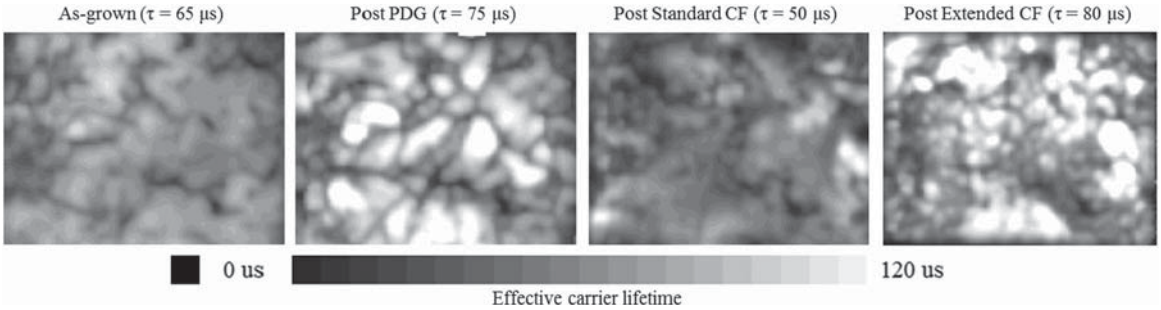

Fig. 1. Effective carrier lifetime mapping μ-PCD of wafers as-grown, post PDG, post standard cofiring (CF), and post extended CF. Lifetime is scaled from 0 to 120 μs. Mean lifetime is indicated above the figures.

Fig. 1 presents the effect of thermal steps during the solar cell fabrication process on bulk lifetime. Neighboring p-type 1.7-Ω·cm multicrystalline (mc) Si wafers of low quality in terms of impurity content are used, with an area of 3×4 cm^2. They have received a $POCl_3$ diffusion obtaining a sheet resistance of 35 $\Omega/\square$, HF dip for phosphorus-silicate glass removal, silicon nitride (SiN_x) plasma-enhanced chemical vapor deposition (PECVD) on the front surface, front Ag-paste, and rear Al-paste screen-printing, and standard or extended cofiring (with a 100-s annealing) in an in-line belt furnace, using similar recipes as the temperature profiles presented in [6]. Reference samples for lifetime measurements follow the process, and after each step, surface layers are etched, chemical cleaning is performed, and fresh SiN_x is deposited on both surfaces to evaluate the bulk quality. Spatially resolved effective carrier lifetime measurements are made using a microwave-detected photoconductance decay (μ-PCD) setup.

Arithmetic mean τ_{eff} of the as-grown wafer is 65 μs. After emitter diffusion (post-PDG sample), τ_{eff} increases above the initial value (75 μs). Experiments confirm that the short 925 °C set temperature spike of 10 s during standard cofiring causes a decrease of postprocessed τ_{eff} (50 μs). However, after using extended cofiring instead of the standard one, mean lifetime measured is well above the value post-PDG (80 μs), thanks to external gettering. This effect can be especially appreciated inside the grains in Fig. 1. Similar results were found studying the phosphorus gettering effect during the cofiring step without using screen-printed metal pastes [5], [6].

Open-circuit voltage (V_{oc}) measurements of the final cells corresponding to the materials shown in Fig. 1 achieved values of 590 mV for a sample with standard cofiring and 595 mV for a sample with extended cofiring. Both V_{oc} values are limited in this experiment by the low-quality mc material and the highly doped emitter that produces high recombination. The 35- $\Omega/\square$ emitter was chosen to maximize the impurity gettering effect during the annealing and to obtain a better contact quality. However, this V_{oc} enhancement is not reflected in efficiency, which is measured to be similar for cells with the extended cofiring and with the standard one. The hypothesis is that in this experiment, the efficiency after extended cofiring was limited by a poor contact because the temperature profile was optimized for gettering effect but not for contacting. Besides the dissolution and gettering of lifetime-killing impurities, the cofiring step must also ensure a low contact resistance, etching uniformly the dielectric and forming Ag crystallites to allow the flow of photogenerated carriers to the contact; in addition, it must avoid p-n-junction shunting by overfiring [14].

The objective of the present work is to study the effect of an annealing performed after the cofiring temperature spike on contact quality and on cell performance and to discuss the possibility of optimizing the temperature profile to include the benefits of a reduction in bulk and emitter recombination.

This aim is approached through the fabrication of simplified Si solar cells using an industrial belt furnace for implementing the extended cofiring of the contacts and characterizing the contact properties for a set of annealing profiles.

III. Material and Methods

Solar cells are processed on 156×156 mm^2, 2-Ω·cm resistivity, 200-μm-thick, p-type boron-doped high-quality mc-Si wafers. After a standard chemical cleaning procedure, a $POCl_3$ diffusion process is carried out obtaining a 30- $\Omega/\square$ sheet-resistance emitter. Then, the front side of the wafers is coated with PECVD silicon nitride. A collection grid is screen-printed with commercial Ag paste on the front side, and Al paste is screen-printed on the rear side. Finally, contact is formed by cofiring the wafers in an infrared belt furnace in air ambient.

Note that selected material—high-quality mc-Si wafers—has been chosen for a more straightforward characterization of the contacting issues associated with the extended cofiring step, although due to its low content of detrimental impurities, it is not most appropriate to see the bulk recombination decrease using the extended cofiring. In addition, note that mc-Si cells are not textured to reduce potential variations due to the step. The highly doped emitter has been selected for improving contact quality and maximizing Ag-crystallite creation, thanks to the presence of a high amount of inactive phosphorous [15]. Although this emitter can limit efficiency values, the main experimental objective is to assure a high-quality contact, and to further analyze the evolution of the contact and the rest of cell parameters during the extended contact cofiring.

The effect of using an extended cofiring instead of the usual standard recipe is studied. Three groups of wafers receive the different time–temperature cofiring profiles represented in Fig. 2. The first recipe corresponds to the standard cofiring, consisting of a first 40-s step, with temperatures between 475 and 600 °C, followed by a temperature peak of 10 s. The second and third

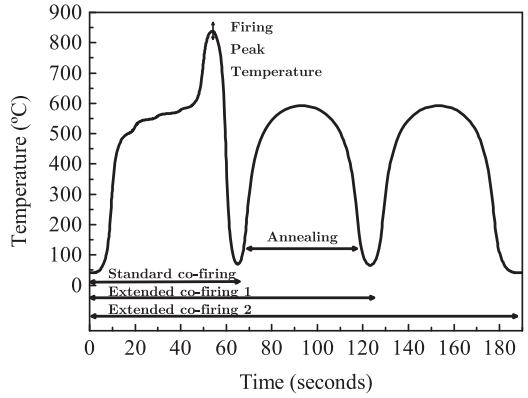

Fig. 2. Set temperature profiles of standard cofiring and variations of extended cofiring 1 and 2.

TABLE I
SOLAR CELL PERFORMANCE MEASURED AT STANDARD CONDITIONS FOR THREE REFERENCE CELLS, EACH ONE WITH COFIRING PROFILE CORRESPONDING TO FIG. 2. FITTED VALUES FOR SHUNT AND SERIES RESISTANCES ARE ALSO SHOWN

Temperature profile	η (%)	FF (%)	V_{oc} (mV)	J_{sc} (mA/cm^2)	R_{shunt} (Ω·cm^2)	R_{series} (Ω·cm^2)
Standard cofiring	15.2	79.4	615	31.1	7283	0.4
Extended cofiring 1	14.8	78.7	613	30.8	11 000	0.6
Extended cofiring 2	14.2	75.4	612	30.8	8330	0.9

recipe correspond to extended cofiring 1 and *2*, respectively, and they consist of a standard cofiring followed by one or two annealing steps at 500–600 °C for 50 s. Maximum annealing time (50 s) is technically limited by belt furnace characteristics that prevent furnace overheating. In terms of impurity behavior, simulations show that the beneficial effect caused by a longer annealing time effect can be similarly obtained by applying subsequent short annealing steps with very fast cooling ramps between them.

Firing set peak temperature of the three recipes is varied between 700 and 880 °C to optimize the extended versions of the cofiring while avoiding to shunt the emitter due to overfiring.

On the one hand, macroscopic characterization of the final cell is performed. Cell parameters are tested using an *I–V* probe station and contact resistance of the front side is measured applying the transfer length method (TLM) [16]. On the other hand, microscopic characterization of the contact is carried out using scanning electron microscopy (SEM) in reference samples after a standard cofiring and an extended cofiring 1. Cross-sectional lamellae samples are previously prepared with *i*n-situ (FIB).

IV. RESULTS AND DISCUSSION

A. Cell Parameters After Different Profile Recipes

Representative results obtained for cell parameters of reference samples using standard cofiring and extended cofiring 1 and 2 with temperature peak of 820 °C are shown in Table I.

It can be observed that implementing an annealing reduces cell efficiency by $-0.4\ \%_{\mathrm{abs}}$ and fill factor by $-0.7\ \%_{\mathrm{abs}}$. When the annealing is performed two times, higher reduction is observed ($-1\ \%_{\mathrm{abs}}$ efficiency and $-4\ \%_{\mathrm{abs}}$ fill factor).

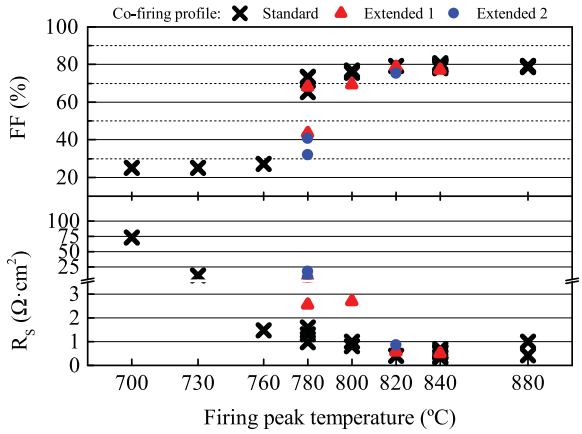

Fig. 3. Measured fill factor and fitted series resistance of cells using different cofiring temperature profiles varying firing peak temperature.

B. Annealing Effect on Series Resistance and Fill Factor

Samples are fired using the three type of recipes shown in Fig. 2, varying in addition peak temperature between 700 and 880 °C. Fig. 3 shows the dependence of measured solar cell fill factor and fitted series resistance on firing peak temperature, representing standard cofiring with black crosses, extended cofiring 1 with red triangles, and extended cofiring 2 with blue dots.

It can be observed that the optimum firing peak temperature for the standard cofiring is 840 °C, using our specific material and processes. Looking at the spike temperatures around the optimum one, series resistance of cells fabricated with the extended cofiring profiles are higher than those obtained with the standard cofiring. Consequently, fill factors using the extended cofiring profiles are lower than those obtained with the standard one. As open-circuit voltage has a mean value of 613 ± 2 mV without correlation with type of cofiring profile (standard or extended) or with spike temperature, fill factor decrease is then related to the series resistance increase. It is important to mention that in the case of highly contaminated wafers, this open-circuit voltage has been experimentally observed to increase due to gettering of highly recombinant impurities (see the example in Section II), but this effect is not evident in this experiment because of the use of lowly contaminated material. In addition, the very highly doped emitter diffusion, selected for improving contact quality, can limit cell performance below the material potential.

Using the standard cofiring (black crosses), we observe series resistance increase and fill factor decrease when peak temperature decreases. This is likely due to the fact that temperature is not high enough to allow the metal paste totally etch the silicon nitride and create silver crystallites during cofiring [1]. After using the extended cofiring recipes 1 and 2 (red triangles and blue dots, respectively), series resistance increases and fill factor decreases when the peak temperature decreases, following the trend observed for the standard cofiring profile, but with worse results when more annealing steps are used. The higher the series resistance after standard cofiring, the worse the deteriorating

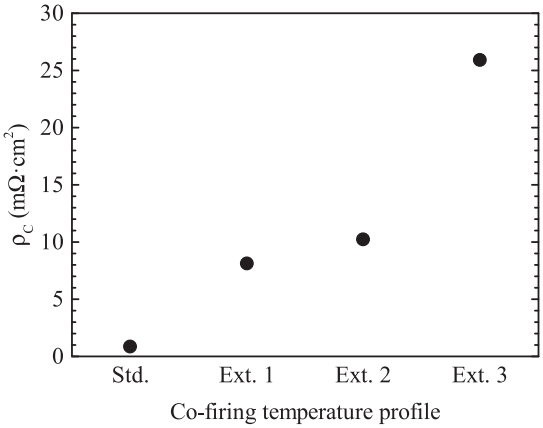

Fig. 4. Specific contact resistance (ρ_c) measured by TLM after standard cofiring (Std.), extended cofiring 1 (Ext. 1), extended cofiring 2 (Ext. 2), and extended cofiring 3 (Ext. 3), which corresponds to a standard cofiring followed by three annealing steps at 600 °C for 50 s. Peak of temperature is 840 °C in all the recipes.

effect of the annealing. Annealing at 600 °C does not contribute to the silicon nitride etching nor the crystallite formation, as can be observed with a series resistance value that does not decrease after annealing. To explain the increased series resistance, the most likely reason is attributed to a growth in thickness of the glass layer appearing at the interface between the metal bulk and silicon [3]. Hypothetically, the worse the initial contact after the temperature spike, the faster the glass layer growth. In addition, a higher series resistance at spike temperatures below the optimum one (840 °C) can also be attributed to an incomplete silicon nitride etching and silver crystallite formation [1].

Additionally, a reduction of the firing peak duration followed by an annealing was tested, with the objective of reducing the thickness of the formed glass layer. However, the metallic belt of the furnace has a thermal inertia that maintains the temperature, and then, in our experiments, solar cell parameters are not sensible to the firing peak duration reduction from 10 to 5 s.

C. Annealing Effect on Specific Contact Resistance

Specific contact resistance (ρ_c) has been measured by TLM after a standard cofiring temperature profile using the optimal firing temperature peak of 840 °C followed by a different number of annealing steps at 600 °C during 50 s each. Fig. 4 shows the results. Using this temperature peak, an optimum specific contact resistance of 0.8 mΩ·cm^2 has been measured that confirms an adequate initial silicon nitride etching and silver crystallite formation.

However, adding annealing steps after the standard cofiring increases ρ_c, measuring a higher increase when the annealing step is repeated. This result is consistent with the increased series resistance reported in the previous section and confirms that it is probably caused by the growth of the interfacial glass layer thickness during 600 °C annealing steps.

D. Scanning Electron Microscopy After Standard and Extended Cofiring

The following are observed and reported in previous studies on current flow paths: 1) direct contact between emitter and

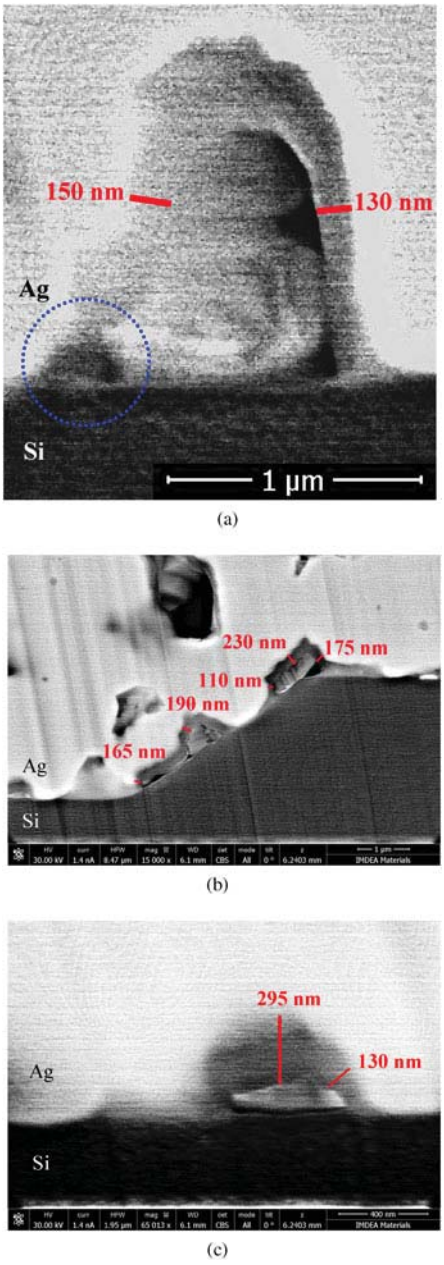

Fig. 5. Cross-sectional SEM images of the contact after standard cofiring (a) and after extended cofiring 1 [(b) and (c)], with the optimum peak temperature of 840 °C. Blue mark corresponds to a direct current path present in the sample after standard cofiring.

Ag-bulk via Ag crystallites or partially covered by a thin (up to a few nanometers) glass layer [17]–[20] and 2) contact through interfacial glass layer richly decorated with nano-Ag colloids [3], [19], [21]. A sample after standard cofiring using the optimal peak temperature of 840 °C and a sample after extended cofiring 1 are measured using SEM. Cross-sectional samples below the metal finger are prepared *in* situ using FIB milling. Fig. 5(a)–(c) shows the results. The contact fired using the standard firing corresponding to Fig. 5(a) shows an Ag crystallite that presents direct contact between silicon and Ag bulk (blue marked) allowing the direct current path.

After annealing [see Fig. 5(b) and (c)], all the crystallites shown in the images are totally surrounded by a thicker glass

layer (>100 nm thick) without presenting direct contact between Ag crystallite and Ag bulk and without an apparent possible nano-Ag colloids path. This glass layer redistribution around the crystallites, without presenting direct current paths—free of interfacial glass layer—most probably causes the measured series resistance increase. A similar correlation of the SEM-measured interfacial glass layer thickness with the increase of series resistance and contact resistance has been also observed in other studies [3], [22], [23]. One possible solution would be to tailor the composition of the paste to avoid the glass layer growth for supporting low-temperature annealing steps below the firing temperature.

E. Consequences for Multicrystalline Silicon Degradation Phenomena

The findings presented above are not only important for cell parameters measured directly after cell processing. It is known from the literature that mc-Si solar cells can degrade under illumination and slightly elevated temperature on a timescale of many hours and days [also called light and elevated temperature-induced degradation (LeTID)], [24], [25]. It is known that high-temperature steps during cell processing are influencing the strength of this degradation, and that they can be minimized by an effective external gettering [26]. It could also be shown that the firing step has a strong influence on LeTID strength, and that it can be minimized by applying a cofiring step at lower temperature [27], [28]. Recently, it could be demonstrated that an additional second firing step at lower peak temperature can significantly reduce the LeTID strength, and it was pointed out that although LeTID can be reduced, cell efficiency (series resistance) might be affected by this second lower temperature firing step [29]. The reason for the possible negative impact on solar cell parameters is not given in [29], but based on our results presented above, we think that a thickening of the glass layer might be the reason for this behavior.

V. Conclusion

The effect of using extended contact cofiring temperature profiles on solar cell performance, in particular on contact formation quality, has been analyzed. Annealing steps after a standard cofiring step increase series resistance and, consequently, decrease fill factor for a range of peak temperatures tested. The lower the peak temperature, the higher the increase of series resistance during annealing. Specific contact resistance measurements using TLM show an increase of this parameter after the annealing steps as compared with the results after the optimal standard recipe. SEM images after standard and extended cofiring steps show a redistribution and thickening of the glass layer surrounding the Ag crystallites during the annealing at low temperature, decreasing the possibility of a current path through direct contact of Ag crystallites with the Ag bulk. This growth of the glass layer can be related to the increase of series resistance and specific contact resistance measured. Degradation of series resistance during the spike temperature, when it is below the optimum one, can also be attributed to an incomplete silicon nitride etching and silver crystallite formation. The beneficial effects on emitter and bulk recombination using extended cofiring demonstrated in previous works require the development of the appropriate metallic screen-printing pastes supporting low-temperature annealing steps without a significant glass layer thickening.

Acknowledgment

A. Peral would like to gratefully acknowledge Dr. M. Castillo and Dr. R. Guzman for their assistance with FIB-SEM measurements at IMDEA Materials and Fellowship for Visiting Scientists Stays (EEBB-I-14-08268 and EEBB-I-15-09198) of the Program for Training of Researchers of the Ministry of Economy and Competitiveness of Spain.

References

[1] G. Schubert, "Thick film metallisation of crystalline silicon solar cells: Mechanisms, models and applications," Ph.D. dissertation, Univ. Konstanz, Konstanz, Germany, 2006.

[2] M. M. Hilali, "Understanding and development of manufacturable screen-printed contacts on high sheet-resistance emitters for low-cost silicon solar cells," Ph.D. dissertation, Georgia Inst. Technol., Atlanta, GA, USA, 2005.

[3] S.-B. Cho, H.-S. Kim, and J.-Y. Huh, "Mechanism underlying the beneficial effect of forming gas annealing on screen-printed Ag contacts of crystalline Si solar cells," *Acta Mater.*, vol. 70, pp. 1–7, May 2014.

[4] V. R. Mehta, "Formation of screen-printed contacts on multicrystalline silicon (MC-Si) solar cells," Ph.D. dissertation, New Jersey Inst. Technol., Newark, NJ, USA, 2010.

[5] J.-F. Leli *et al.*, "Dissolution and gettering of iron during contact co-firing," *Energy Procedia*, vol. 8, pp. 257–262, 2011.

[6] A. Peral, J. F. Lelièvre, F. Recart, and C. del Cañizo, "Defect engineering during the contact co-firing step in an industrial belt furnace," *Phys. Status Solidi (c)*, vol. 9, nos. 10/11, pp. 2107–2110, Oct. 2012.

[7] B. Michl, J. Schön, W. Warta, and M. Schubert, "The impact of different diffusion temperature profiles on iron concentrations and carrier lifetimes in multicrystalline silicon wafers," *IEEE J. Photovoltaics*, vol. 3, no. 2, pp. 635–640, Apr. 2013.

[8] D. Macdonald, A. Cheung, and A. Cuevas, "Gettering and poisoning of silicon wafers by phosphorus diffused layers," in *Proc. 3rd World Conf. Photovoltaic Energy Convers.*, 2003, vol. 2, pp. 1336–1339.

[9] A. E. Morishige *et al.*, "Building intuition of iron evolution during solar cell processing through analysis of different process models," *Appl. Phys. A*, vol. 120, no. 4, pp. 1357–1373, Jul. 2015.

[10] M. Rinio *et al.*, "Improvement of multicrystalline silicon solar cells by a low temperature anneal after emitter diffusion," *Prog. Photovoltaics, Res. Appl.*, vol. 19, no. 2, pp. 165–169, Mar. 2011.

[11] J. Hofstetter *et al.*, "Enhanced iron gettering by short, optimized low-temperature annealing after phosphorus emitter diffusion for industrial silicon solar cell processing," *Phys. Status Solidi (c)*, vol. 8, no. 3, pp. 759–762, 2011.

[12] J. Schön, H. Habenicht, M. C. Schubert, and W. Warta, "Understanding the distribution of iron in multicrystalline silicon after emitter formation: Theoretical model and experiments," *J. Appl. Phys.*, vol. 109, no. 6, 2011, Art. no. 063717.

[13] A. Dastgheib-Shirazi *et al.*, "Dissolution of electrically inactive phosphorus by low temperature annealing," *Energy Procedia*, vol. 77, pp. 286–290, Aug. 2015.

[14] I. B. Cooper *et al.*, "Understanding and use of IR belt furnace for rapid thermal firing of screen-printed contacts to Si solar cells," *IEEE Electron Device Lett.*, vol. 31, no. 5, pp. 461–463, May 2010.

[15] E. Cabrera *et al.*, "Impact of excess phosphorus doping and Si crystalline defects on Ag crystallite nucleation and growth in silver screen-printed Si solar cells: Impact of emitter and crystal defects on Si solar cell Ag metallization," *Prog. Photovoltaics, Res. Appl.*, vol. 23, no. 3, pp. 367–375, Mar. 2015.

[16] D. L. Meier and D. K. Schroder, "Contact resistance: Its measurement and relative importance to power loss in a solar cell," *IEEE Trans. Electron Devices*, vol. ED-31, no. 5, pp. 647–653, May 1984.

[17] C. Ballif, D. M. Huljić, G. Willeke, and A. Hessler-Wyser, "Silver thick-film contacts on highly doped n-type silicon emitters: Structural and electronic properties of the interface," *Appl. Phys. Lett.*, vol. 82, no. 12, 2003, Art. no. 1878.

[18] S. Kontermann, R. Preu, and G. Willeke, "Calculating the specific contact resistance from the nanostructure at the interface of silver thick film contacts on n-type silicon," *Appl. Phys. Lett.*, vol. 99, no. 11, 2011, Art. no. 111905.

[19] P. Kumar *et al.*, "Combined microstructural and electrical characterization of metallization layers in industrial solar cells," *Energy Procedia*, vol. 67, pp. 31–42, Apr. 2015.

[20] R. Hoenig *et al.*, "The nature of screen printed front side silver contacts—Results of the project MikroSol," *Energy Procedia*, vol. 43, pp. 27–36, 2013.

[21] Z. G. Li, L. Liang, and L. K. Cheng, "Electron microscopy study of front-side Ag contact in crystalline Si solar cells," *J. Appl. Phys.*, vol. 105, no. 6, 2009, Art. no. 066102.

[22] M. M. Hilali *et al.*, "Effect of glass frit chemistry on the physical and electrical properties of thick-film Ag contacts for silicon solar cells," *J. Electron. Mater.*, vol. 35, no. 11, pp. 2041–2047, Nov. 2006.

[23] S. Kontermann *et al.*, "Physical understanding of the behavior of silver thick-film contacts on n-type silicon under annealing conditions," *Sol. Energy Mater. Sol. Cells*, vol. 93, no. 9, pp. 1630–1635, Sep. 2009.

[24] K. Ramspeck *et al.*, "Light induced degradation of rear passivated mc-Si solar cells," in *Proc. 27th Eur. Photovoltaic Sol. Energy Conf. Exhib.*, Frankfurt, Germany, 2012, pp. 861–865.

[25] F. Kersten *et al.*, "Degradation of multicrystalline silicon solar cells and modules after illumination at elevated temperature," *Sol. Energy Mater. Sol. Cells*, vol. 142, pp. 83–86, Nov. 2015.

[26] A. Zuschlag, D. Skorka, and G. Hahn, "Degradation and regeneration in mc-Si after different gettering steps," *Prog. Photovoltaics, Res. Appl.*, 2016, to be published.

[27] D. Bredemeier, D. Walter, S. Herlufsen, and J. Schmidt, "Lifetime degradation and regeneration in multicrystalline silicon under illumination at elevated temperature," *AIP Adv.*, vol. 6, no. 3, Mar. 2016, Art. no. 035119.

[28] K. Nakayashiki *et al.*, "Engineering solutions and root-cause analysis for light-induced degradation in p-type multicrystalline silicon PERC modules," *IEEE J. Photovoltaics*, vol. 6, no. 4, pp. 860–868, Jul. 2016.

[29] C. E. Chan *et al.*, "Rapid stabilization of high-performance multicrystalline p-type silicon PERC cells," *IEEE J. Photovoltaics*, vol. 6, no. 6, pp. 147–1479, Nov. 2016.